RESEARCH PAPER

Freezing strain characteristics and mechanisms of unsaturated frozen soil: analysis of matric suction and water–ice phase change

Huie Chen[1] · Hua Du[1] · Haotian Guo[1] · Fansheng Kong[1] · Zhongqiong Zhang[2]

Abstract

The freezing strain characteristics of unsaturated soil are quite different from those of saturated soil. Besides the commonly observed frost heave, unsaturated soil may also experience frost shrinkage, causing uneven surface deformation and deterioration of soil properties. Matric suction and water–ice phase change are key factors affecting the freezing strain characteristics of soil. In this study, the freezing strain characteristics and underlying mechanisms of lean clay samples with different initial matric suctions at varying temperatures were investigated. A mathematical relationship between soil temperature and matric suction was established, enabling the estimation of variation trends in matric suction. The internal mechanisms of different freezing strain characteristics were analyzed based on the mesoscopic structures of frozen samples with low and high initial matric suctions. The results showed that samples with low initial matric suction and frozen at low negative temperatures are prone to frost heave. Frost heave occurs when the volume expansion of the soil caused by water–ice phase change exceeds the volume reduction due to increased matric suction; otherwise, frost shrinkage occurs. The morphology of pore ice in samples with different initial matric suctions varies, reflecting the degree of water–ice phase change in the soil. Using the Pearson correlation coefficient method, an empirical model for axial freezing strain applicable to unsaturated frozen lean clay was established, and the model's validity was confirmed with experimental data.

Keywords Freezing strain · Matric suction · Mesoscopic structure · Unfrozen water · Unsaturated frozen soil

✉ Huie Chen
   chenhe@jlu.edu.cn

   Hua Du
   huadu21@mails.jlu.edu.cn

   Haotian Guo
   guohaotian@163.com

   Fansheng Kong
   kongfs21@mails.jlu.edu.cn

   Zhongqiong Zhang
   zhongqionghao@163.com

[1]   College of Construction Engineering, Jilin University, Changchun 130026, China

[2]   State Key Laboratory of Frozen Soil Engineering, Northwest Institute of Eco-Environment and Resources, Chinese Academy of Science, Lanzhou 730000, China

1 Introduction

Frozen soil is globally widespread, covering approximately 50% of the total land area [43, 49]. Under certain conditions such as rainfall, transpiration, and freeze–thaw cycles, the moisture field within the soil undergoes dynamic changes [44, 48], leading to alterations in soil saturation states [18]. During freezing, the complex interactions among soil particles, air, and water lead to variations in matric suction and water–ice phase changes. These processes contribute to distinct deformation features for soil with different saturation degrees, specifically frost heave and frost shrinkage [23, 29, 30, 41, 46, 47]. The rearrangement of soil particles caused by freezing changes the soil structure [35], and affects its strength [19], permeability [34], and heat conductivity [43]. These variations have significant implications for the stability of engineering structure, regional topographic feature, and hydrological conditions, potentially leading to geotechnical disasters [25].

Researchers have investigated the characteristics of soil frost heave and analyzed the effects of certain factors on this phenomenon. Some studies have examined the impact of particle size distribution on frost heave sensitivity in coarse-grained soils [7, 12–14, 31]. Teng et al. [29] proposed a novel criterion for assessing soil frost heave sensitivity using analytical solutions. Zhang et al. [40], Lai et al. [16], and Li et al. [17] carried out unilateral freezing experiments on saline soil and silty clay, examining the influence of salt content and water heat transfer on soil frost heave. Bai et al. [6] discovered a critical threshold for the effect of initial water content on water–vapor migration and frost heave in unsaturated soils. Existing research indicated a direct correlation between soil frost heave and boundary temperature, as well as soil–water and soil-freezing characteristics.

The development of micro-meso testing techniques, such as computerized tomography (CT) [9, 33, 39], scanning electron microscope (SEM) [27, 37, 42], and image processing methodologies, has paved the way for revealing soil freezing strain mechanisms at the micro-meso level. Watanabe et al. [36] employed a CDD camera with micron-level resolution to observe the microstructure of the soil near the freezing front. Their findings indicated that the growth rate of the ice lens increases with increased freezing speed. Arenson et al. [3, 4] used a high-resolution camera to investigate the ice segregation process in silt during freezing, and utilized particle image velocimetry technology to observe the growth of ice crystals and soil displacement. Zhou et al. [50] captured the freezing process of clay with a high-resolution microscope and observed the growth process of segregated ice in the soil. Therefore, modern techniques provide an effective means to explore the soil freezing process from a mesoscopic perspective [26].

Current research primarily focuses on discussing soil freezing strain characteristics concerning frost heave at negative temperatures, leaving a gap in the exploration of soil frost shrinkage. During freezing, soil deformation is closely related to its unsaturated properties, specifically matric suction. So the investigation of the freezing strain characteristics of soil from the perspective of matric suction and the revelation of its underlying mechanisms hold significant theoretical and practical importance for tackling geotechnical challenges in frozen soil regions.

In this study, the lean clay from Changchun, a city in China's seasonally frozen region, was taken as the research object. Indoor freezing experiments were conducted to determine the freezing strain characteristics of the soil samples, considering variations in initial matric suction and freezing temperature. The soil–water characteristic curve (SWCC) and soil freezing characteristic curve (SFCC) of the sample were explored using a pressure plate apparatus and a nuclear magnetic resonance system, respectively. Additionally, the mesoscopic structure of frozen samples with low and high initial matric suctions was observed by a laser confocal microscope. The objective is to explain the mechanisms of water–ice phase changes and matric suction influencing soil freezing strain characteristics from perspectives of unfrozen water content and ice morphology. Based on the experimental results, an empirical model of axial freezing strain was established for lean clay samples with different initial matric suctions and experienced different negative temperatures.

2 Materials and methods

2.1 Soil properties and sample preparation

The lean clay was collected from Changchun City, China. The sampling area has a semi-humid and semi-arid continental monsoon climate. It is a typical seasonally frozen region characterized by dry and windy spring, hot and rainy summer, and cold and dry winter conditions.

The sampling sites are shown in Fig. 1. The groundwater level fluctuates notably between wet and dry seasons, with depths ranging from approximately 4.10 to 5.80 m. Lean clay serves as the main aquifer, with evaporation exceeding precipitation. The freezing period is from November to April of the next year (Fig. 1b). The freezing depth ranges from 1.50 to 1.80 m.

The XY-100 engineering rig was used for sampling, with a sampling depth ranging from 5.00 to 6.00 m. The undisturbed soil samples obtained have a diameter of 10 cm and a height of 20 cm. In their natural state, the soil displays plasticity and a yellow–brown color, as shown in Fig. 2a.

The mineral composition of the soil was analyzed by the TTR III multifunctional X-ray diffractometer. The results indicate that quartz and feldspar constitute the main primary minerals, accounting for approximately 60.0% of the total content. Additionally, illite–smectite mixed-layer and illite are the predominant secondary minerals, comprising approximately 35.0% of the total content. The mineral composition of the soil is illustrated in Fig. 2b.

Granulometric analysis was performed on the soil samples, and the results are depicted in Fig. 2c. The solid black line in Fig. 2c is the grading curve expressed by the average particle size. The soil predominantly consists of silt and clay particles, corresponding to 61.0% and 34.0%, respectively. Further, Fig. 2d illustrates the test results for the water content and density, with average values of 26.33% and 1.89 g/cm^3, respectively. It is evident that the material composition and fundamental physical properties among the sampled soils are essentially consistent.
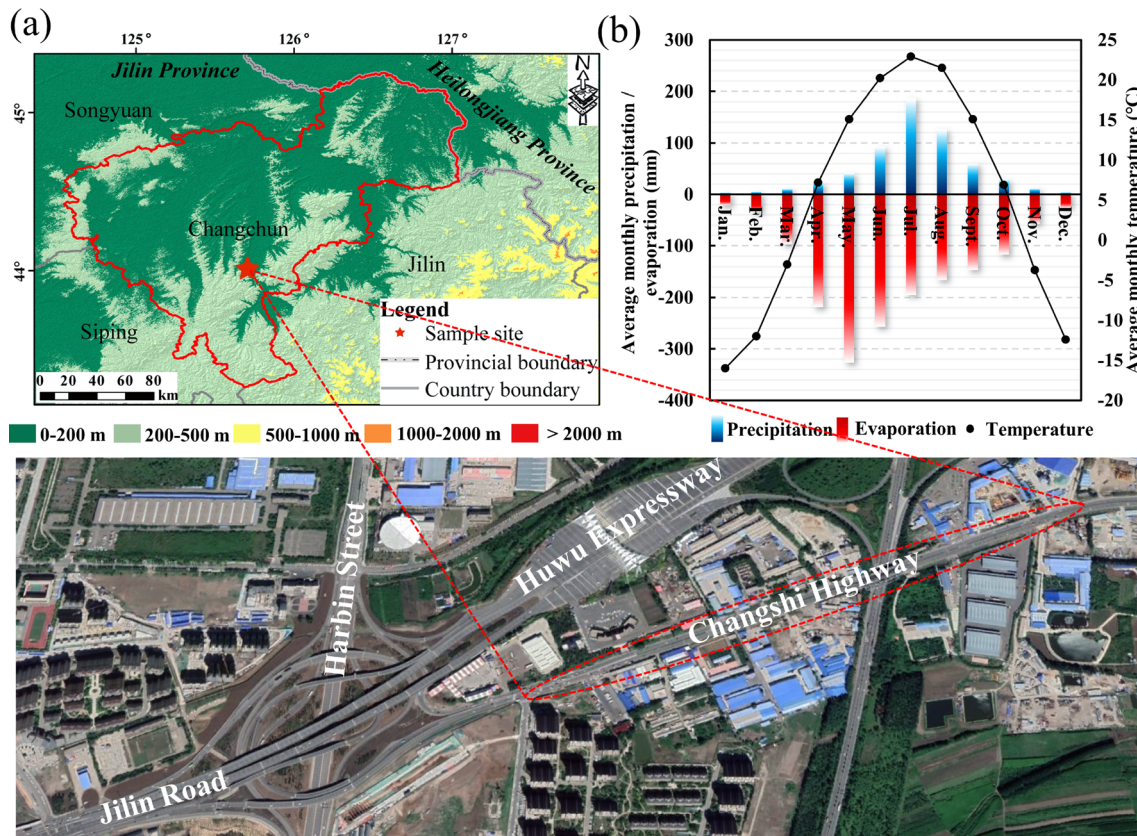
Fig. 1 The sampling sites

The other physical properties of the soil are shown in Table 1, representing the average values for the parameters. The natural saturation degree is 87.6%, with a corresponding matric suction of 57 kPa (measured by the GEO-Experts pressure plate instrument). Therefore, in the subsequent experiments, the initial matric suction conditions of the samples were set as 57 kPa, 100 kPa, 200 kPa, 300 kPa, and 400 kPa, corresponding to saturation degrees of 87.6%, 72.0%, 64.8%, 60.3%, and 57.7%, respectively.

The soil contains a total soluble salt content of 0.015%, classifying it as non-saline soil. Therefore, when considering the unsaturated characteristics, the effect of osmotic suction formed by ionic composition can be ignored. The suction mentioned here is matric suction.

Initially, undisturbed soil samples were cut into cylinder samples with dimensions of $\Phi 38$ mm $\times$ 76 mm (Fig. 3(1)). The GDS unsaturated soil triaxial apparatus was then employed to set the initial matric suction for the samples at 57 kPa, 100 kPa, 200 kPa, 300 kPa, and 400 kPa, as illustrated in Fig. 3(2). During the freezing test process, these samples were placed in a cooling apparatus, and the axial and radial strains of the samples frozen under

different negative temperatures were measured using dial indicators (Fig. 3(3)). As depicted in Fig. 3(4) and (5), following the freezing test, the frozen samples with initial matric suctions of 57 kPa and 400 kPa were sliced for mesoscopic structure examinations under negative temperatures. For the unfrozen water content test, cylinder samples ($\Phi 38$ mm $\times$ 76 mm) with different initial matric suctions were further cut into cylinder samples measuring 60 mm in height and 25 mm in diameter, as illustrated in Fig. 3(6), to match the size requirements of the NMR system (Fig. 3(7)). When measuring the soil–water characteristics, undisturbed samples were cut into ring knife samples with dimensions $\Phi 70$ mm $\times$ 20 mm (Fig. 3(8)). Saturation was then achieved (Fig. 3(9)), and a pressure plate apparatus was employed to simulate the dehumidification process (Fig. 3(10)). Except for the mesoscopic structure examination samples, other samples were prepared under constant room temperature, which took a relatively short time with minimal air–water exchange. Therefore, changes in water content (saturation degree or matric suction) during this process could be ignored. The sampling preparation procedure is shown in Fig. 3.
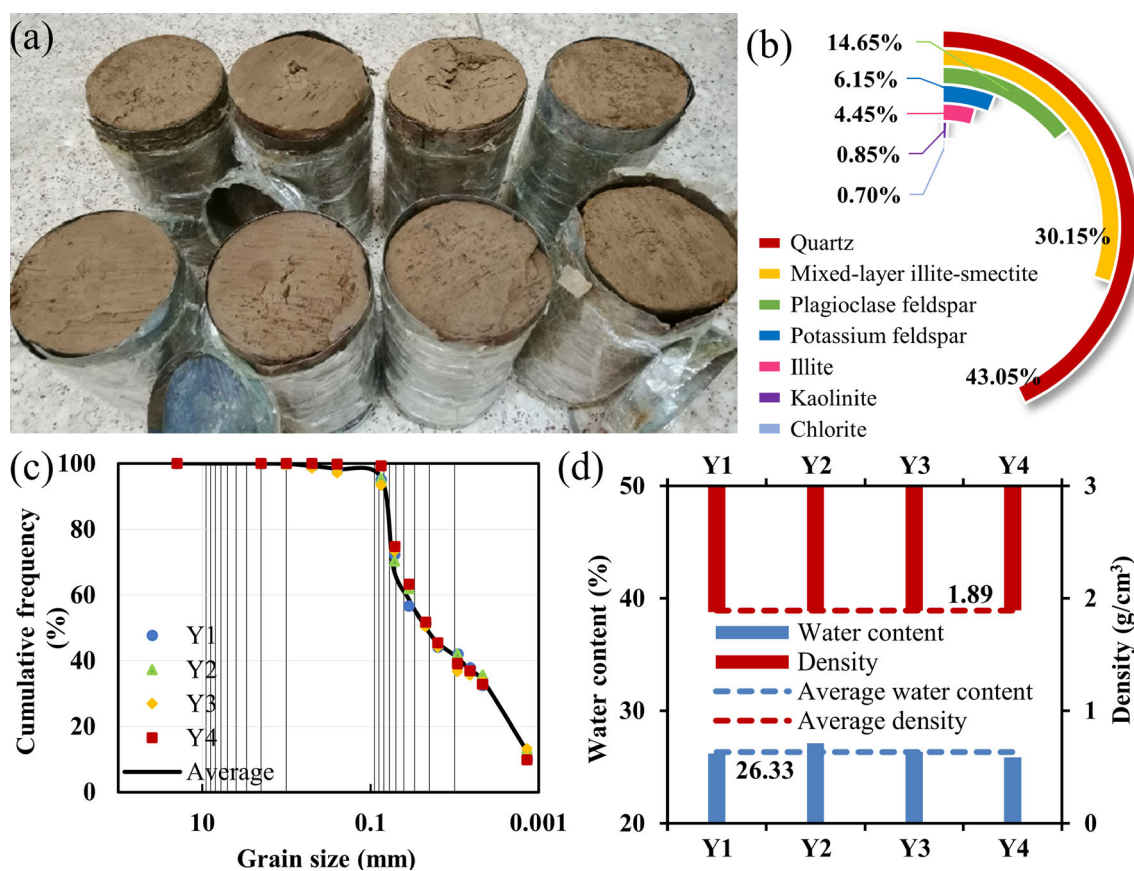
Fig. 2 Properties of the lean clay obtained by drilling

Table 1 The average value of physical properties of lean clay. Saturation, Liquid Limit and Plastic Limit should be rounded to one decimal point to reflect correctly the accuracy

Specific gravity	Saturation degree (%)	Void ratio	Liquid limit (%)	Plastic limit (%)
2.72	87.56	0.82	38.77	24.61

2.2 Apparatus and experimental procedure

2.2.1 Freezing strain test

The freezing strain characteristics of samples under different negative temperatures were tested by the YTZ-C freezing–thawing test machine and dial indicators (Fig. 4). The apparatus has a temperature control range of $\pm 20.0°$C, with a precision of 0.2°C. Strains were measured by four dial indicators, each with a range of 20 mm and an accuracy of 0.01 mm. These indicators, as shown in Fig. 4b and c, were positioned to measure both axial and radial strains of the samples during freezing.

The freezing temperatures were set to -5°C, -10°C, and -15°C. At the beginning of the test, record the initial readings of the dial indicators, and when the temperature

reaches the designed value, readings were taken at 5 min, 10 min, 30 min, 1 h, 2 h, 3 h, 4 h, 8 h, and 12 h. Photographs were taken to record the readings. This process was brief and had little impact on the freezing test. The freezing strain of the samples stabilized after 12 h (the dial indicator reading changing less than 0.01 mm for three consecutive hours). The difference between the stable reading and the initial reading was taken as the final strain value. The average of the final strain values measured by the three dial indicators was taken as the radial strain. To verify the test results, soil samples with different initial matric suctions underwent step cooling to -10°C and then -15°C after finishing the freezing process at -5°C, with the aforementioned test procedures repeated. The freezing strain test procedure is shown in Fig. 5.

2.2.2 Soil–water characteristics test

The soil–water characteristics of unfrozen samples were tested using the GEO-Experts pressure plate instrument. The saturated ring knife sample was placed inside the instrument, and matric suction was applied to simulate dehumidification. Considering that the maximum air entry value of the clay plate is 500 kPa, the suction range was set
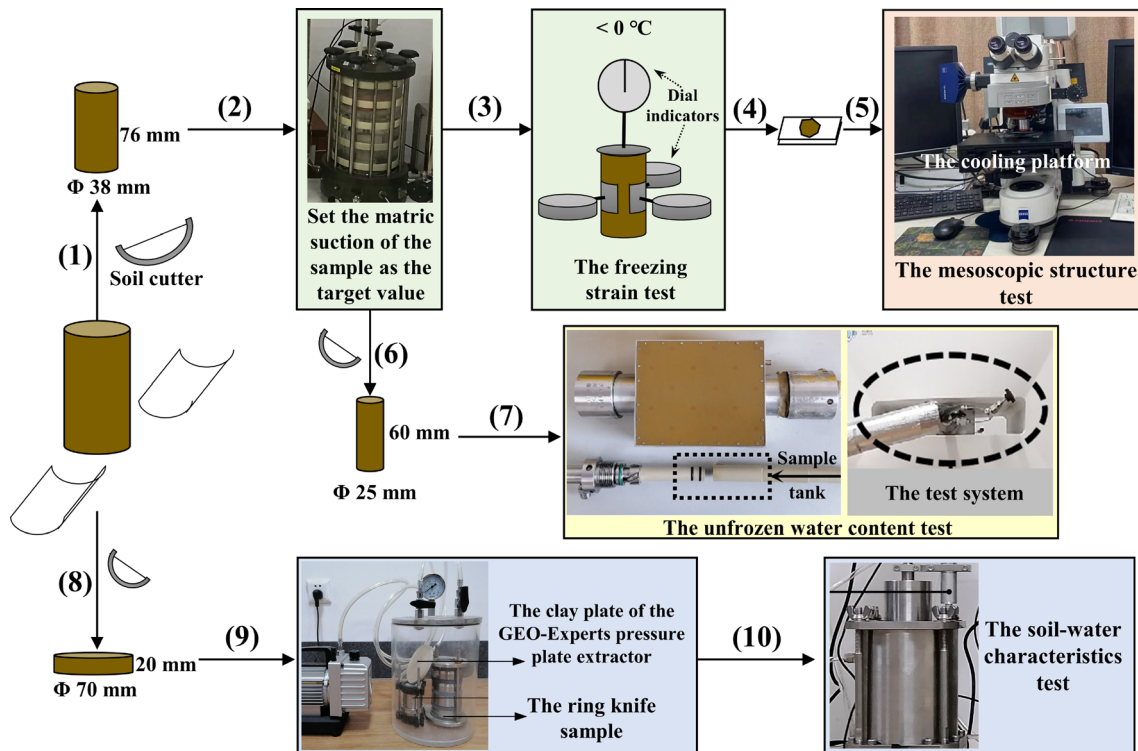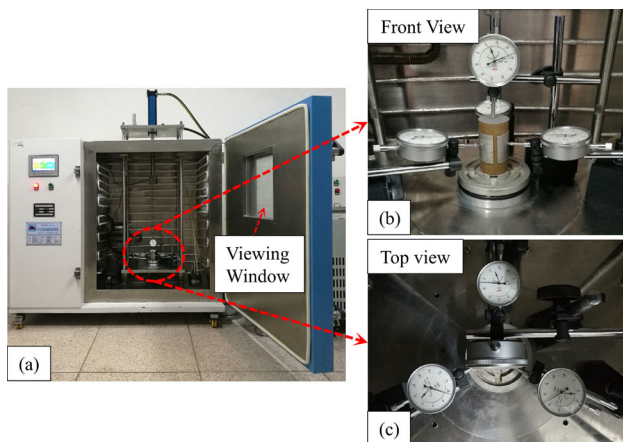
Fig. 3 The sample preparation procedure

Fig. 4 The YTZ-C freezing–thawing test machine and dial indicators

from 0 to 475 kPa, with 22 levels (Table 2). The pressure plate instrument was considered balanced at the current matric suction level when the displacement volume within 48 h did not exceed 0.05 ml. At this point, the next suction level was applied [36].

2.2.3 Unfrozen water characteristics test

The unfrozen water content in the samples was tested by the MesoMR23-060H-I multifunctional NMR analysis and imaging system, which has a temperature control range from − 40.0 to 99.0°C and an accuracy of 0.1°C.

Based on the average monthly temperature of Changchun, twelve temperatures from − 17 to 15°C were selected to investigate the variation of unfrozen water content (volume water content) in samples with different initial matric suctions. To ensure the accuracy of the test results, the samples underwent both cooling and subsequent heating. The NMR signal stabilized after 1 h of freezing. Therefore, the NMR signal measured after the temperature reached the target value and remained constant for 1 h was used to calculate the unfrozen water content.

2.2.4 Mesoscopic structure test

The Zeiss LSM700 laser confocal microscope was employed to observe the mesoscopic structure of the sample frozen under constant negative temperature. It is equipped with a cooling platform system (Fig. 3) capable of real-time temperature control. The cooling platform utilizes liquid nitrogen for cooling, with a minimum temperature of − 196.0°C and a temperature control accuracy of 0.1°C. The scanning resolution ranges from 4 × 1 to 2048 × 2048, and the z-axis resolution is 10 nm, with an 18 mm diagonal scanning field.
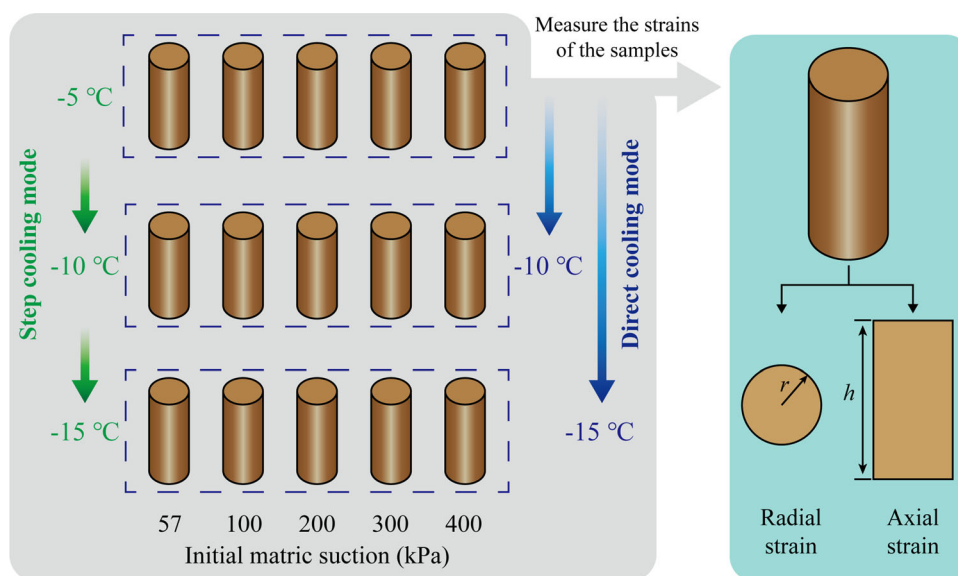
Fig. 5 Freezing strain test procedure (Note: In the step cooling mode, the same sample is cooled to − 10°C after completing the test at − 5°C, and then cooled to − 15°C for further test after completing the test at − 10°C; in the direct cooling mode, different samples are direct-cooled to − 5°C, − 10°C, or − 15°C)

Table 2 Procedure for soil–water characteristics test

Level	Matric suction (kPa)	Level	Matric suction (kPa)
1	5	12	225
2	10	13	250
3	15	14	275
4	25	15	300
5	50	16	325
6	75	17	350
7	100	18	375
8	125	19	400
9	150	20	425
10	175	21	450
11	200	22	475

3 Results and discussion

3.1 Freezing strain characteristics

The axial and radial strains of the samples during the freezing process are shown in Fig. 6. The freezing strains observed in the step cooling process are similar to those in the direct cooling mode, confirming the accuracy of the test results. Positive strains indicate frost heave, while negative strains signify frost shrinkage.

Figure 6a shows that the axial strain of the sample with low initial matric suction is positive with a maximum value of 1.46%. As the initial matric suction increases, frost heave gradually decreases. When the initial matric suction is 400 kPa, axial frost shrinkage occurs at − 5°C and − 10°C. The radial strain transitions from positive to negative with increasing initial matric suction. The most significant radial frost shrinkage occurs at − 10°C. The radial frost heave is observed only when the initial matric suction is 57 kPa. Both maximum axial frost heave and frost shrinkage exceed the radial ones.

Figure 7 shows the variations of axial and radial strains with temperature during the freezing process. It can be seen that under different negative temperatures, samples with varying initial matric suctions exhibit similar freezing strain characteristics. Samples with initial matric suctions ranging from 57 to 300 kPa display positive axial strains, indicating frost heave. The magnitude of axial frost heave decreases with increasing temperature. The sample with an initial matric suction of 400 kPa shows axial frost shrinkage at − 5°C and frost heave at − 15°C. The sample with an initial matric suction of 57 kPa consistently exhibits positive radial strains. Conversely, the sample with an initial matric suction of 400 kPa consistently displays negative radial strains, with absolute values initially increasing and subsequently decreasing as the temperature decreases. Since the sample's axial size is twice that of its radial size, temperature changes prompt a higher degree of pore water migration and freezing along the axial direction than in the radial direction. Additionally, the radial and axial freezing strains of the sample affect each other. Therefore, the following analysis of freezing strain focuses on the axial strain.
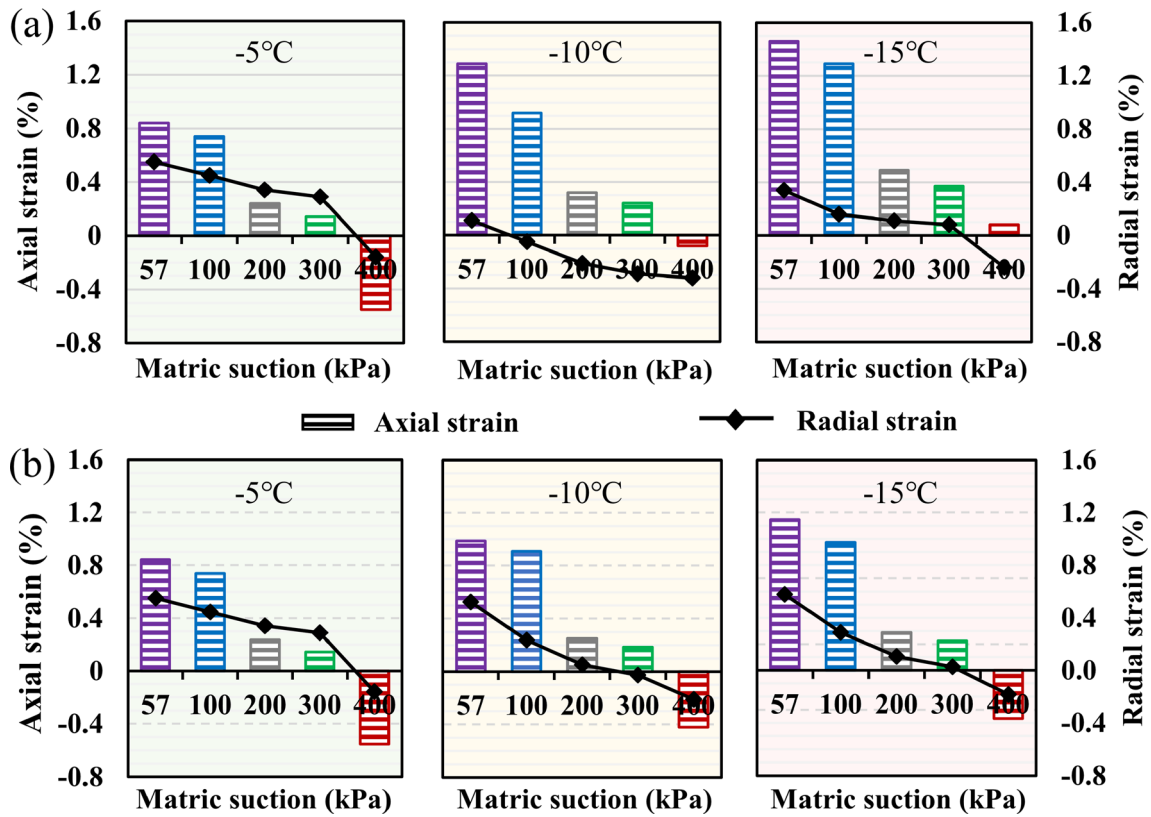
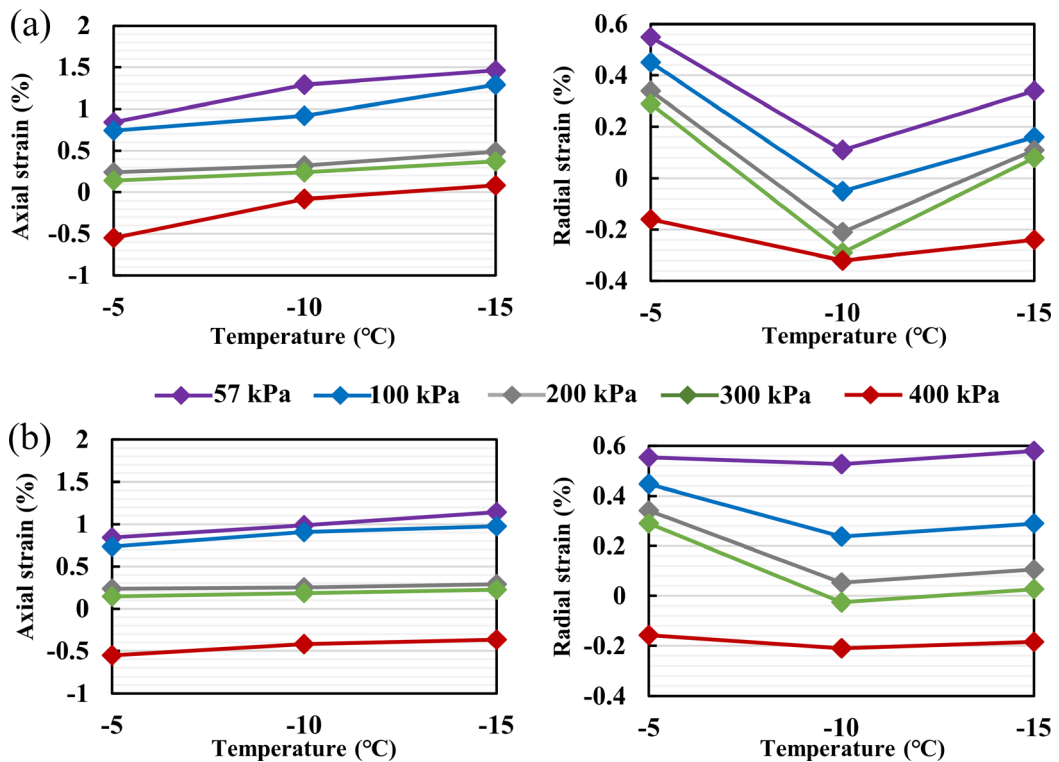Fig. 6 Variation of freezing strains with initial matric suction: **a** Direct cooling and **b** step cooling modes

Fig. 7 Variation of freezing strains with temperature: **a** Direct cooling and **b** step cooling modes

3.2 Water distribution characteristics

According to the above analysis, when the temperature was step-cooled to − 15 °C, both axial and radial strains of the sample with the initial matric suction of 400 kPa showed negative values, indicating frost shrinkage. To further investigate the mechanism of soil frost shrinkage, the water content of the central and marginal parts of this sample was determined before and after the freezing process. The accuracy of the results was confirmed by testing six samples, as depicted in Fig. 8a.

Figure 8a shows that after step-cooling to − 15°C, the water content in the central part of the samples uniformly decreases, and most of that in the marginal part decreases, except for a slight increase in Sample 4. During the freezing process, pore water in the sample migrates from the warmer and lower matric potential part (center) to the colder and higher matric potential part (margin) under the combined action of temperature and matric potential, inducing the decrease of the water content inside the sample. The water content change in the marginal part is the result of both water migration and ice sublimation [21] after the water–ice phase change (Fig. 8b). Ice sublimation reduces the resistance to particle movement, thus facilitating soil particle displacement.

3.3 Unfrozen water content characteristics

3.3.1 Results of unfrozen water content test

Figure 9 illustrates the variation of unfrozen water content in the samples during the cooling and heating process. It can be found that, under positive temperatures, the unfrozen water content decreases with increasing matric suction. Furthermore, samples with identical initial matric suction maintain nearly consistent unfrozen water content under the same temperature during the cooling and heating process, confirming the reliability of the test results. In addition, the unfrozen water content in the samples showed a similar trend: decreasing during the cooling process and subsequently increasing during the heating process. During the cooling process, a portion of the water in the sample starts to freeze at the freezing point, forming an ice-water mixture. However, before reaching about − 2.2°C, there is little change in the unfrozen water content. This phenomenon arises due to supercooling, wherein the reduction in system free energy hinders the crystallization and nucleation of free water [8, 45, 47]. As the temperature continues to decline from − 2.2 to − 7°C, the unfrozen water content in the sample decreases rapidly, signifying rapid freezing of water within the sample at this stage. When the temperature drops to − 17°C, loosely bound water freezes slowly, while strong bound water keeps unfrozen, leading to a stabilized unfrozen water content. The freezing and thawing of pore water exhibit hysteresis due to differences in the thermal dynamic potential energy of water. This results in the preferential freezing of water in large pores and the prior melting of ice in small pores, preventing overheating phenomena during the thawing process. Moreover, the melting of ice in small pores requires pre-melting on the ice surface. Therefore, the unfrozen water content in the samples under the same temperature during the freezing and thawing process is not completely consistent, with a notable hysteresis observed in the increase of unfrozen water content during thawing.
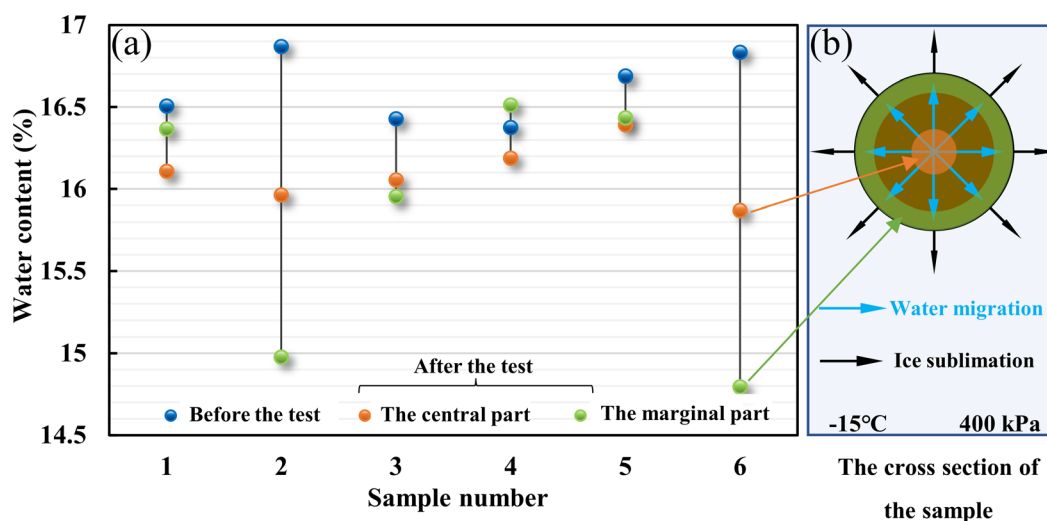

Fig. 8 Variation of water content of the samples with initial matric suction of 400 kPa before and after the freezing process: **a** Test results and **b** schematic
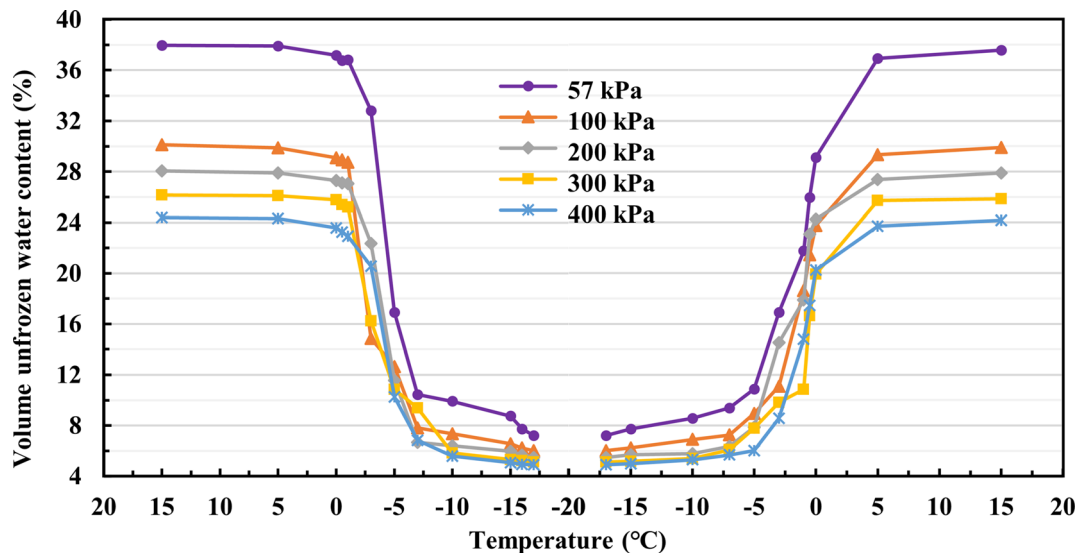
Fig. 9 Variation of unfrozen water content in samples with different initial matric suction during the freezing and thawing process

3.3.2 Fitting model of SFCC

The test results of unfrozen water content allow the establishment of SFCC, which relates volume unfrozen water content to temperature [32]. Numerous empirical formulas have been put forward to describe the variation of unfrozen water content with temperature, primarily falling into four categories: linear function, power function, exponential function, and piecewise function. Among these, the power function fitting model developed by Anderson and Tice [2] and Anderson and Morgenstern [1] (Eq. (1)) stands out as the most widely utilized, demonstrating both feasibility and practical effectiveness.

$$\theta_u = \alpha |T|^\beta \tag{1}$$

where, θ_u is the volume unfrozen water content in %; T is the freezing temperature in °C; α and β are empirical parameters related to the specific surface area and liquid limit of the soil, which can be determined by fitting SFCCs. Based on Eq. (1), Xu et al. [38] proposed a prediction model for unfrozen water content (Eq. (2)). This model offers a clear physical meaning for the empirical parameters in Eq. (1) and solves the problem of dimensional inconsistency between the left and right sides of the formula. Therefore, the optimized power function fitting formula is used here.

$$\theta_u = \theta_0 \left(\frac{T}{T_f}\right)^k \tag{2}$$

where, θ_0 is the initial volume water content in %; T_f is the initial freezing temperature in °C, marking the point where pore water starts to freeze into ice when T is less than T_f. k represents the slope of the curve, serving to characterize

the freezing rate of soil pore water, which can be determined by the fitting curve.

Based on the test data of unfrozen water content, fitting curves were obtained (Fig. 10). These curves effectively characterize the experimental data, except in the range of − 2 to 0°C. According to the test results, the initial freezing temperature of the studied sample is determined to be − 2.2°C. In the temperature range of − 2.2 to 0°C, the system experiences supercooling, and the volume unfrozen water content only changes when the temperature drops below − 2.2°C. Therefore, it is reasonable to observe a relatively large dispersion in the fitting curves within the − 2 to 0°C range. The fitting parameter k, elaborated in Table 3, is set at − 0.55 in this work.

3.3.3 Effect of unfrozen water content on freezing strain

Based on the results of freezing strain and unfrozen water content tests, the curves depicting the relationship between axial strain and unfrozen water content of samples are shown in Fig. 11. It can be seen that, under the same negative temperature, the unfrozen water content increases with the decrease of initial matric suction. With the decreasing unfrozen water content, axial frost heave increases while axial frost shrinkage decreases. The axial strain of samples with an initial matric suction ranging from 57 to 300 kPa is positive, indicating frost heave. When the initial matric suction is 400 kPa, the axial strain is positive at − 15°C, decreases with increasing unfrozen water content, and reaches − 0.55% at − 5°C.

Figure 12 illustrates the variations of unfrozen water content and frozen water content of samples with initial matric suction and freezing temperatures. Frozen water
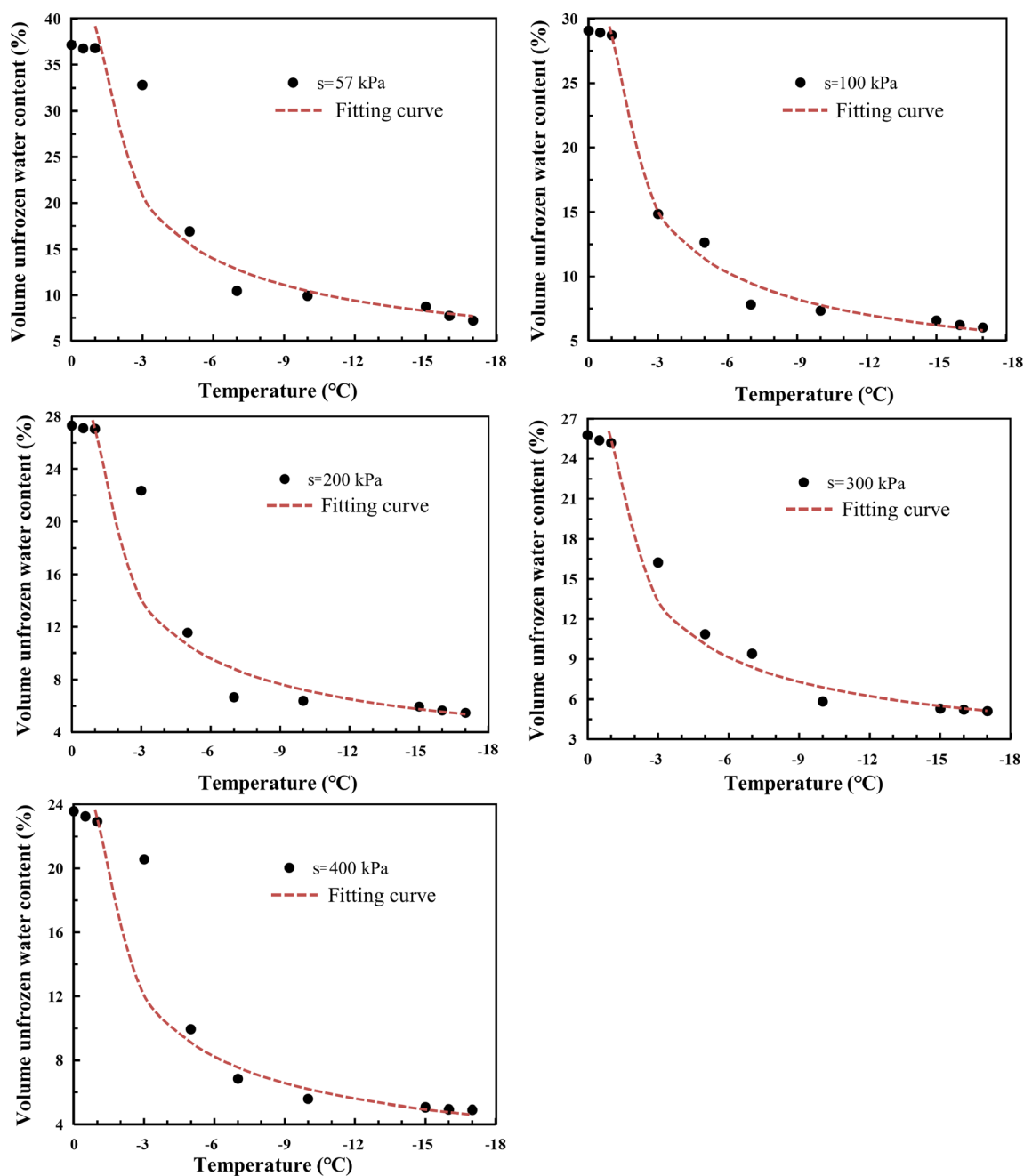
Fig. 10 The power function fitting model of SFCC

Table 3 Parameters of the power function fitting model

Fitting parameter	Initial matric suction (kPa)				
	57	100	200	300	400
k	− 0.529	− 0.571	− 0.557	− 0.550	− 0.554
R^2	0.91	0.98	0.92	0.97	0.93

content represents the amount of water that completes the water–ice phase change under negative temperatures. It is calculated as the difference between the initial water content and the unfrozen water content.

In Fig. 12, as the freezing temperature decreases under constant initial matric suction, the soil's unfrozen water content decreases while the frozen water content increases. This results in an expansion in sample volume due to the increasing degree of water–ice phase change. For the sample with an initial matric suction of 400 kPa, the unfrozen water content reaches its maximum value at − 5°C, while concurrently, the frozen water content
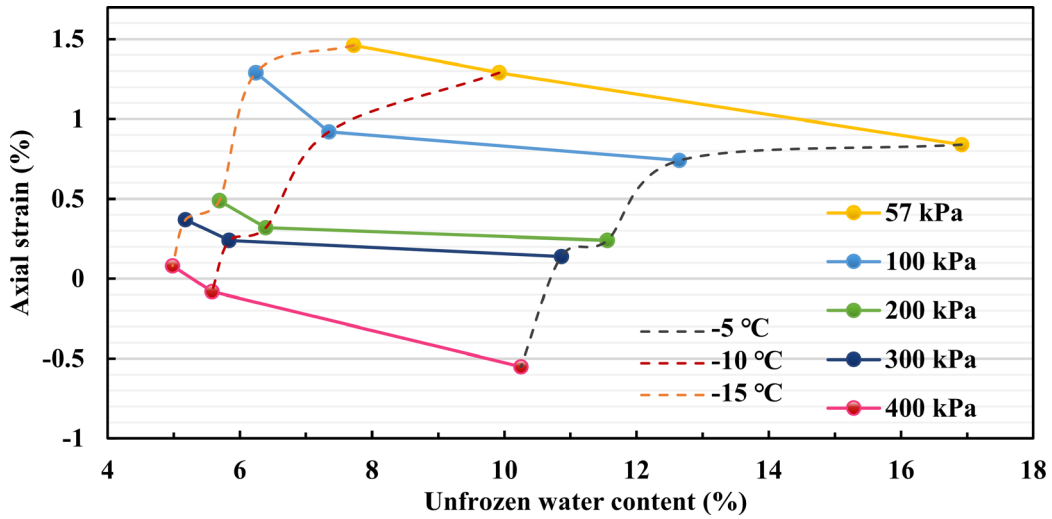
Fig. 11 Variation of axial strain with unfrozen water content of samples with different initial matric suction
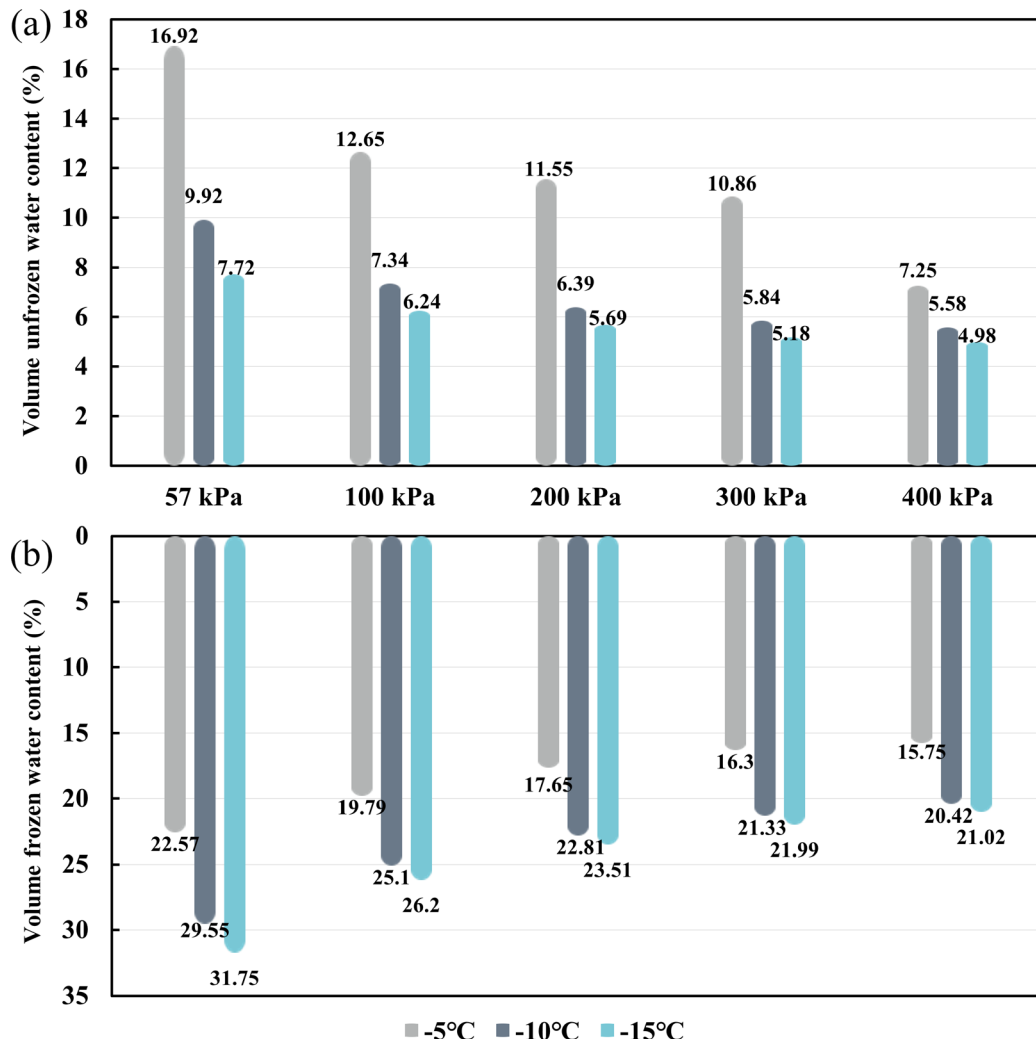

Fig. 12 Volume water content in samples with different initial matric suction and experienced different negative temperatures: **a** Volume unfrozen water content and **b** volume frozen water content

reaches its minimum value. At this time, the sample experiences a low degree of water–ice phase change, resulting in an axial freezing strain of -0.55%, indicating frost shrinkage. When the temperature is $-15°C$, the frozen water content increases by 33.46% compared to that at $-5°C$, indicating a higher degree of water–ice phase change. This increase leads to a greater volume expansion of the sample, transforming frost shrinkage into weak frost heave, with a corresponding axial freezing strain of 0.08%. In addition, under constant freezing temperatures, the initial water content of the sample decreases with increasing initial matric suction. Both the unfrozen water content and frozen water content of samples with high initial matric suction are lower than those of samples with low initial matric suction. Therefore, as the degree of water–ice phase change inside the soil decreases, axial frost heave decreases while axial frost shrinkage increases.

3.4 Matric suction characteristics

In this section, the matric suction of samples frozen under different negative temperatures was estimated. The variation of matric suction in the frozen samples with initial matric suction and temperature was studied. Additionally, the relationship between matric suction and sample freezing strain was analyzed.

3.4.1 SWCC of unfrozen samples

The experimental procedure for the soil–water characteristic test is detailed in Sect. 2.2.2. Based on the displacement volume obtained under each level of matric suction, the relationship between volume water content and matric suction is established, as plotted in Fig. 13. It can be seen that the saturated volume water content of the lean clay sample is 43.4%. Due to equipment limitations, the residual volume water content of the sample cannot be directly measured. However, its value can be derived by a fitting model based on experiment results [28]. It can be seen from Fig. 13 that the volume water content of the sample decreases with increasing matric suction, and the air entry value is about 25 kPa.

The SWCC is fitted by the classical van Genuchten (VG) model (Eq. (3)) [11], and the results are shown in Fig. 13. The fitting parameters and determination coefficients are provided in Table 4.

$$\theta_\omega = \theta_r + \frac{\theta_s - \theta_r}{\left[1 + (as)^q\right]^{\left(1 - \frac{1}{q}\right)}} \tag{3}$$

where, θ_ω, θ_r, and θ_s are the volume water content, residual volume water content, and saturated volume water content

of the sample, respectively, in %; s is the matric suction in kPa; a and q are the fitting parameters.

3.4.2 Matric suction of frozen samples

Since the 1960s, researchers have delved into the similarities between SWCC and SFCC, providing corresponding theoretical explanations [10, 15, 20, 24]. Ma et al. [22] and Watanabe et al. [36] compared the theoretical results of matric suction obtained by inverse analysis of the SFCC and the measured results. Though some differences were observed, the theoretical results were found to reasonably capture the changing trend of actual matric suction to some extent.

Therefore, neglecting the differences in surface tension between the water–air and water–ice interfaces [15], the trend of matric suction with temperature can be determined based on the VG model of SWCC (Eq. (3)) and the optimized power function fitting model of SFCC (Eq. (2)), as shown in Eq. (4). The parameters in this formula have been described in the previous section. Using Eq. (4), the matric suction of samples frozen under different negative temperatures can be determined. This allows for the analysis of the relationship between matric suction and freezing strain characteristics.

$$s = \frac{1}{a}\left[\left(\frac{\theta_s - \theta_r}{\theta_0\left|\frac{T}{T_f}\right|^k - \theta_r}\right)^{\frac{1}{1-\frac{1}{q}}} - 1\right]^{\frac{1}{q}} \tag{4}$$

The matric suction of samples frozen under different negative temperatures can be obtained by substituting the initial volume water content of the samples into Eq. (4), as illustrated in Fig. 14. Under a constant initial matric suction, the matric suction of the frozen samples increases with decreasing temperature. As shown in Fig. 12, the decrease in temperature leads to an increase in frozen water content and a decrease in unfrozen water content in the samples, resulting in an increase in matric suction. In addition, under the same temperature, the matric suction of frozen samples increases with the increasing initial matric suction. This is because samples with high matric suction have a low initial water content, and after freezing, the unfrozen water content in these samples further decreases, causing an increase in matric suction.

3.4.3 Effect of matric suction on freezing strain

Figure 15 illustrates the relationship between matric suction and axial strain of samples. It can be seen that under the same temperature, the magnitude of frost heave decreases with the increase of matric suction. Specifically,
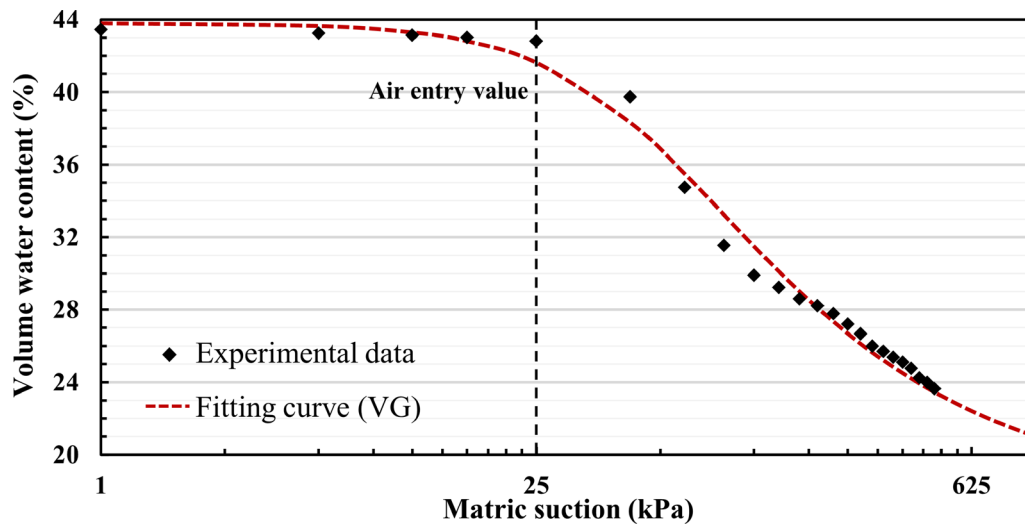
Fig. 13 The SWCC of the lean clay sample

Table 4 Fitting parameters of the SWCC

Fitting parameters	a (kPa^{-1})	q	θ_s(%)	θ_r(%)	R^2
Value	0.017	1.698	43.81	17.34	0.993

at $-5°C$ and $-10°C$, samples with an initial matric suction of 400 kPa show axial frost shrinkage. The rise in matric suction increases interparticle force, facilitating a reduction of soil volume. For the sample with an initial matric suction of 400 kPa, the matric suction after freezing is significantly higher than that before freezing. At this time, the freezing strain of the soil sample is primarily influenced by the enhanced interparticle force produced by the increased matric suction, resulting in frost shrinkage.

The matric suction after freezing increases with decreasing temperature under a constant initial matric suction, which typically leads to volume reduction of the sample. However, there is an observed increase in axial frost heave and a decrease in frost shrinkage. The result indicates that frost shrinkage does not necessarily occur under high matric suction, as supported by Fig. 16. To be exact, the final freezing strain characteristics of the soil are determined by a combination of matric suction and water–ice phase change degree. As the freezing temperature decreases, the frozen water content increases, causing a high degree of water–ice phase change in the soil. This, in turn, prompts an expansion in the sample volume. When the volume reduction of the soil caused by increased matric suction is not sufficient to offset the volume expansion induced by the water–ice phase change, frost heave occurs. Therefore, axial frost heave increases with decreasing temperature under constant initial matric suction.
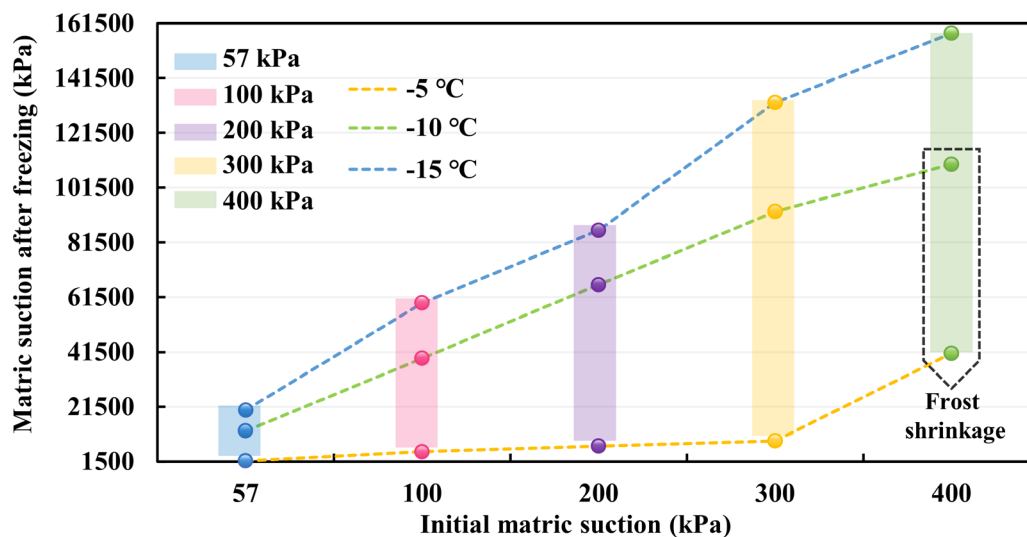

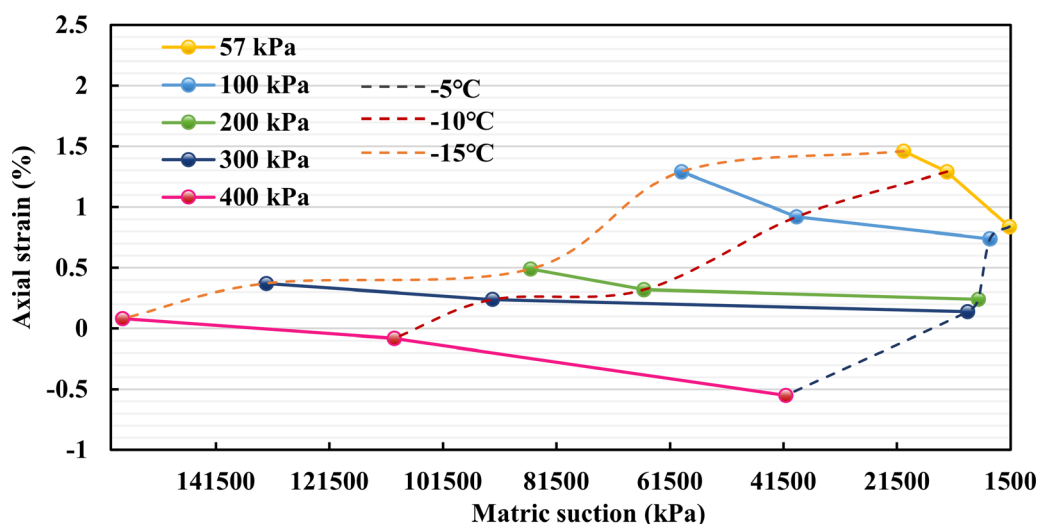**Fig. 14** Variation of matric suction of samples frozen under different negative temperatures

Fig. 15 Variation of axial strain with matric suction of samples frozen under different temperatures
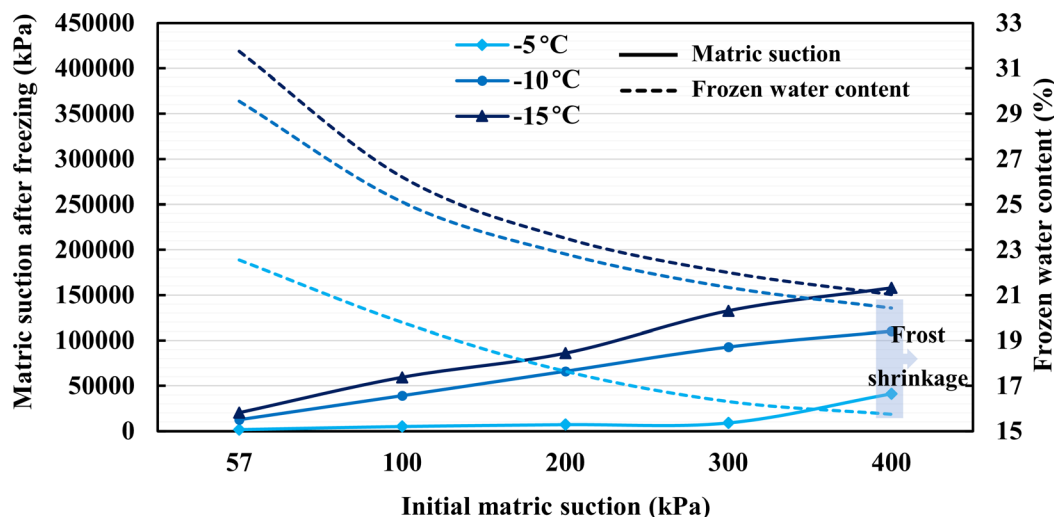

Fig. 16 Variation of matric suction and frozen water content of samples with initial matric suction under different negative temperatures

3.5 The mesoscopic structure characteristics

According to the freezing strain test results, upon step-cooling to − 15°C, samples with an initial matric suction of 57 kPa exhibited positive axial and radial strains, indicating frost heave. Conversely, samples with an initial matric suction of 400 kPa displayed negative axial and radial strains, indicating frost shrinkage. In order to explore the mesoscopic mechanisms governing freezing strain characteristics, sliced samples from the freezing strain tests were prepared. The mesostructures of samples, with initial matric suctions of 57 kPa and 400 kPa, were scanned using the Zeiss LSM700 laser confocal microscope. The results are shown in Fig. 17a and b. It can be seen that significant

ice formation occurs in both samples under negative temperatures, but the ice morphology is different.

Under low initial matric suction (57 kPa), pore ice typically forms as strips and flakes, enveloping soil particles with larger crystals or thin film, as shown in Fig. 17a. At this time, the frozen water content, the degree of water–ice phase change, and the volume expansion induced by the phase change from water to ice are high. Although the matric suction increases due to water–ice phase change, it remains considerably smaller than that observed in samples indicating frost shrinkage with an initial matric suction of 400 kPa. The effect of the increased interparticle force is not significant. Thus, the soil freezing strain is primarily influenced by the expansion caused by the water–ice phase change, resulting in overall frost heave.
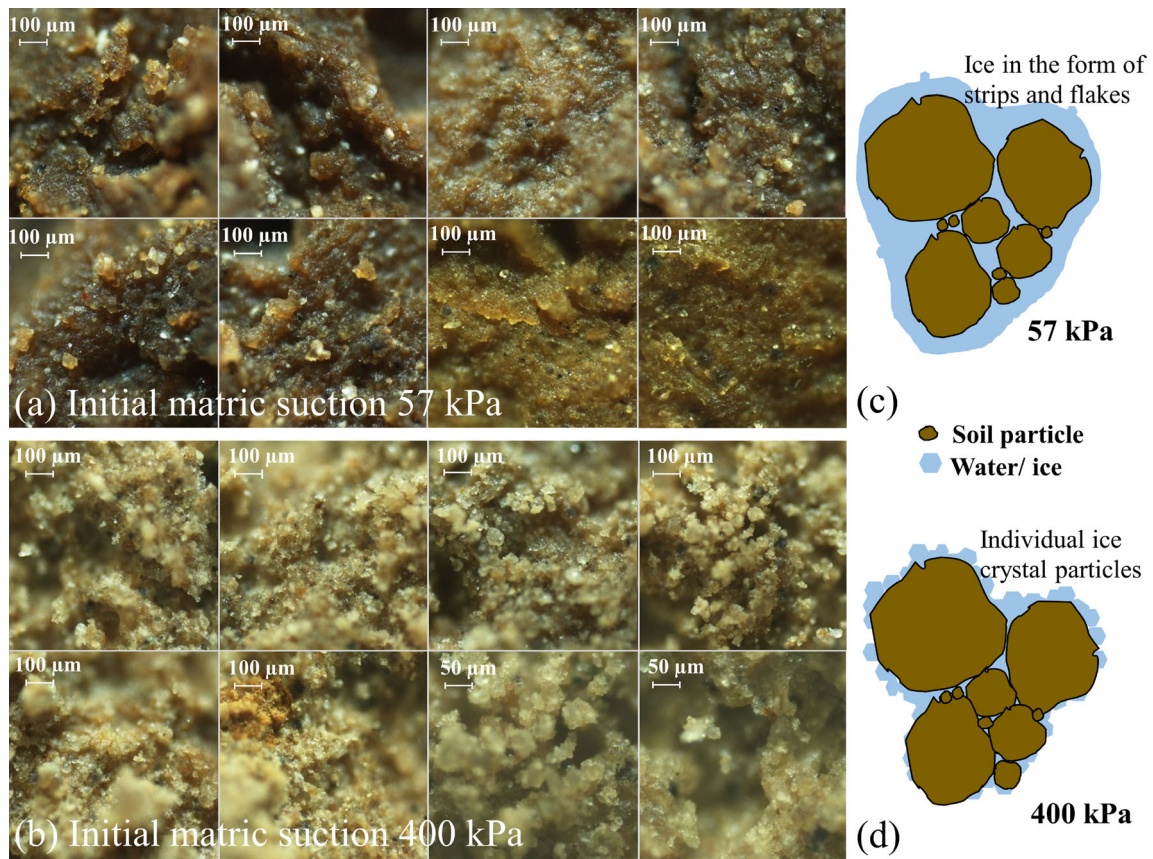
Fig. 17 Mesoscopic structure and freezing strain mechanism of samples with low (57 kPa) and high (400 kPa) initial matric suctions when step-cooling to − 15°C

In the sample with high initial matric suction (400 kPa), pore ice primarily exists as individual ice crystals. Soil particles in the sample are not entirely enveloped by ice crystals but are predominantly connected to them at certain points and planes, as shown in Fig. 17b. Upon step-cooling to − 15 °C, the initial water content, frozen water content, and degree of water–ice phase change are low, resulting in small soil volume expansion. Meanwhile, some water freezes into ice under negative temperatures, causing an increase in matric suction. Increased interparticle forces compress soil particles together. Frost shrinkage primarily results from the soil volume reduction due to increased matric suction, outweighing the effect of soil volume expansion caused by water–ice phase change. In addition, ice crystals formed under high initial matric suction are easier to sublimate compared to the thin film ice produced under low initial matric suction. This significantly reduces resistance to soil particle movement, making the soil more prone to frost shrinkage. The mechanism is illustrated in Fig. 17c and d.

3.6 An empirical model for axial freezing strain

As discussed earlier, the freezing strain characteristics of the samples are influenced by factors such as initial matric suction, unfrozen water content, and matric suction after freezing. Herein, the Pearson correlation analysis method was used to study the relationship between axial freezing strain and these factors, and the findings are summarized in Table 5.

Table 5 reveals a notable correlation between the axial freezing strain of the sample and the initial matric suction. As described earlier, the freezing strain characteristics are determined by both the matric suction and the degree of

Table 5 Pearson correction analysis results between axial freezing strain and influencing factors

	Initial matric suction	Unfrozen water content	Matric suction after freezing
Correlation coefficient	− 0.90**	0.24	− 0.39

The presence of ** indicates a significant correlation at the 0.01 level
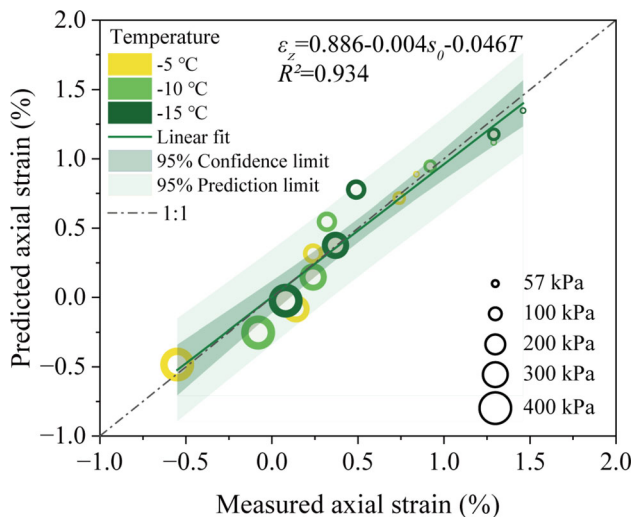
Fig. 18 Comparison between predicted and measured results

water–ice phase change. When the volume expansion caused by water–ice phase change is greater than the volume reduction caused by increased matric suction, it shows frost heave; otherwise, it indicates frost shrinkage. With a fixed initial matric suction, the matric suction and the degree of water–ice phase change in the frozen sample are determined by the freezing temperature. Based on this, an empirical formula is established to predict the axial freezing strain of lean clay samples under different freezing temperatures:

$$\varepsilon_z = 0.886 - 0.004s_0 - 0.046T \tag{5}$$

where, ε_z is the axial strain in %; s_0 is the initial matric suction in kPa; T is the freezing temperature in °C. The determination coefficient R^2 of Eq. (5) is 0.934.

Figure 18 illustrates the relationship between the predicted axial freezing strain values, calculated by Eq. (5), and the experimental data. It is evident that the empirical model developed in this study accurately reflects the variation in axial freezing strain of unsaturated lean clay samples with initial matric suction under different temperatures. This model can be effectively employed for predicting freezing strain characteristics in such soils.

4 Conclusions

In this study, the freezing strain characteristics of unsaturated soil were investigated under different initial matric suctions and freezing temperatures. The internal mechanisms of frost heave and frost shrinkage of the soil were explained from the perspectives of unfrozen water content, variations in matric suction, and mesoscopic structure. The following conclusions are mainly obtained:

1. The freezing strain characteristics of the soil are determined by both the volume expansion caused by the water–ice phase change and the volume reduction induced by increased matric suction.

2. Under constant initial matric suction, the degree of water–ice phase change in the soil decreases as unfrozen water content increases, resulting in reduced soil volume expansion. Higher initial matric suction and lower freezing temperatures induce an increase in matric suction, leading to a reduction in sample volume.

3. At low initial matric suction, a significant water–ice phase change occurs, leading to ice in strips and flakes. Conversely, at high initial matric suction, the degree of water–ice phase change is low, and ice dominantly exists in crystals. The ice morphology serves as a direct indicator of the soil's water–ice phase change degree.

4. Through correlation analysis, the initial matric suction and freezing temperature are found to determine the freezing strain characteristics of the soil. The established empirical model can effectively reflect the variation of axial freezing strain of unsaturated lean clay with initial matric suction and freezing temperature.

Constrained by instrumental limitations, the freezing strain of unsaturated soil samples has not been examined under higher initial matric suction and lower freezing temperatures. Subsequent research may involve expanding the experiment parameter range and dataset to further investigate the freezing strain characteristics and underlying mechanisms of the samples. The empirical model could then be refined based on these insights.

Author contributions Huie Chen: Writing, reviewing, project administration. Hua Du: Conceptualization, writing-original draft preparation. Haotian Guo: Validation, methodology. Fansheng Kong: Validation, visualization. Zhongqiong Zhang: Project administration.

Data availability The datasets generated during and/or analyzed during the current study are available from the corresponding author on reasonable request.

Declarations

Conflict of interest The authors declare that they have no known competing financial interests or personal relationships that could have appeared to influence the work reported in this study.

References

1. Anderson DM, Morgenstern NR (1974) Physics, chemistry, and mechanics of frozen ground: a review. Int J Rock Mech Min Sci Geomech Abs 11(8):A165

2. Anderson DM, Tice AR (1972) Predicting unfrozen water contents in frozen soils from surface area measurements. Hwy Res Record 393:12–18

3. Arenson LU, Azmatch TF, Sego DC, Biggar KW (2008) A new hypothesis on ice lens formation in frost-susceptible soils. Int Conf Permafrost Proc 9:59–64

4. Arenson LU, Sego DC, Take WA.(2007) Measurement of ice lens growth and soil consolidation during frost penetration using particle image velocimetry (PIV). Ottawa. Canadian Geotechnical Society., p. 2046–2053.

5. ASTM C1699–09. Standard test method for moisture retention curves of porous building materials using pressure plates. 2009.

6. Bai R, Lai Y, Zhang M, Ren J (2020) Study on the coupled heat-water-vapor-mechanics process of unsaturated soils. J Hydrol 585:124784

7. Bilodeau JP, Dore G, Pierre P (2008) Gradation influence on frost susceptibility of base granular materials. Int J Pavement Eng 9(6):397–411

8. Buoyoucos G (1920) Degree of temperature to which soils can be cooled without freezing. J Agric Res 20:267–269

9. Chen SJ, Ma W, Li GY (2019) Study on the mesostructural evolution mechanism of compacted loess subjected to various weathering actions. Cold Reg Sci Tech 167:102846

10. Flerchinger GN, Seyfried MS, Hardegree SP (2006) Using soil freezing characteristics to model multi-season soil water dynamics. Vadose Zone J 5(4):1143–1153

11. Van Genuchten MT (1980) A closed-form equation for predicting the hydraulic conductivity of unsaturated soils. Soil Sci Soc Am J 44(5):892–898

12. Hao X, Ma W, Feng W, Wen Z, Zhang L, Gao Y (2023) Discussion on the frost susceptibility of sandy soil under hydraulic pressure. Cold Reg Sci Tech 211:103860

13. Konrad JM (2008) Freezing-induced water migration in compacted base-course materials. Can Geotech J 45(7):895–909

14. Konrad JM, Lemieux N (2005) Influence of fines on frost heave characteristics of a well-graded base-course material. Can Geotech J 42(2):515–527

15. Koopmans RWR, Miller RD (1966) Soil freezing and soil water characteristic curves. Soil Sci Soc Am Proc 30:680–685

16. Lai Y, Pei W, Zhang M, Zhou J (2014) Study on theory model of hydro-thermal–mechanical interaction process in saturated freezing silty soil. Int J Heat Mass Transf 78:805–819

17. Li S, Zhang M, Pei W, Lai Y (2018) Experimental and numerical simulations on heat-water-mechanics interaction mechanism in a freezing soil. Appl Therm Eng 132:209–220

18. Lin B, Zhang F, Feng D, Tang K, Feng X (2017) Accumulative plastic strain of thawed saturated clay under long-term cyclic loading. Eng Geol 231:230–237

19. Liu J, Chang D, Yu Q (2016) Influence of freeze-thaw cycles on mechanical properties of a silty sand. Eng Geol 210:23–32

20. Liu Z, Zhang B, Yu X, Zhang B, Tao J. A new freezing method for soil water characteristic curve measurement. Conference A new freezing method for soil water characteristic curve measurement.

21. Lu Y, Liu S, Weng L, Wang L, Li Z, Xu L (2016) Fractal analysis of cracking in a clayey soil under freeze–thaw cycles. Eng Geol 208:93–99

22. Ma TT, Wei CF, Zhou JZ, Tian HH (2015) Freezing characteristic curves and water retention characteristics of soils. Chin J Geotech Eng 37(S1):172–177 ((in Chinese))

23. Nitao JJ, Bear J (1996) Potentials and their role in transport in porous media. Water Resour Res 32(2):225–250

24. Spaans EJA, Baker JM (1996) The soil freezing characteristic: its measurement and similarity to the soil moisture characteristic. Sci Soc Am J 60(1):13–19

25. Sun K, Zhou A (2021) A multisurface elastoplastic model for frozen soil. Acta Geotech 16(11):3401–3424

26. Takeda K, Okamura A (1997) Microstructure of freezing front in freezing soils. International Symposium Ground Freezing Frost Action Soils. Lulea, Sweden. p. 171-178.

27. Tang YQ, Yan JJ (2014) Effect of freeze–thaw on hydraulic conductivity and microstructure of soft soil in Shanghai area. Environ Earth Sci 73(11):7679–7690

28. Tao GL, Li J, Zhuang XS, Xiao HL, Cui XL, Xu WS (2018) Determination of the residual water content of SWCC based on the soil moisture evaporation properties and micro pore characteristics. Rock Soil Mech 39(04):1256–1262 ((in Chinese))

29. Teng J, He H, Feng X, Yan H, Zhang S (2023) A novel criterion for assessing frost heave susceptibility of soils. Acta Geotech 19:2233–2249

30. Tuller M, Or D, Dudley LM (1999) Adsorption and capillary condensation in porous media: Liquid retention and interfacial configurations in angular pores. Water Resour Res 35(7):1949–1964

31. Vinson TS, Ahmad F, Rieke R (1986) Factors important to the development of frost heave susceptibility criteria for coarse-grained soils. Transp Res Rec.124–31.

32. Vu QH, Pereira J-M, Tang AM (2022) Effect of fines content on soil freezing characteristic curve of sandy soils. Acta Geotech 17(11):4921–4933

33. Wang Z, Fu S, Zhao X, Jiang W, Liu G, Li D et al (2024) Modeling temperature change and water migration of unsaturated soils under seasonal freezing-thawing conditions. Cold Reg Sci Technol. 218:104074

34. Wang T, Liu Y, Wang J, Wang D (2020) Assessment of spatial variability of hydraulic conductivity of seasonally frozen ground in Northeast China. Eng Geol 274:105741

35. Wang D, Ma W, Niu Y, Chang X, Wen Z (2007) Effects of cyclic freezing and thawing on mechanical properties of Qinghai-Tibet clay. Cold Reg Sci Tech 48(1):34–43

36. Watanabe K, Mizoguchi M, Ishizaki T, Fukuda M (1997) Experimental study on microstructure near freezing front during soil freezing. Trans Jpn Soc Irrig Drain Reclam Eng 191:633–638

37. Wen D, Jiang N, Liu C, Lv Z (2023) Study of the influence of temperature rise on the microstructure of frozen soil based on SEM and MIP. J Mater Civil Eng. 35(5):05023001

38. Xu X, Oliphant JL, Tice AR (1985) Prediction of unfrozen water content in frozen soil by a two-point or one-point method. Proc 4th Int Symp Ground Freezing.2:83–87.

39. Ye W, Li C (2018) The consequences of changes in the structure of loess as a result of cyclic freezing and thawing. Bull Eng Geol Environ 78(3):2125–2138

40. Zhang J, Lai Y, Zhao Y, Li S (2020) Study on the mechanism of crystallization deformation of sulfate saline soil during the uni-directional freezing process. Permafrost Periglac 32(1):102–118

41. Zhang Z, Li M, Wen Z, Yin Z, Tang Y, Gao S et al (2023) Degraded frozen soil and reduced frost heave in China due to climate warming. Sci Total Environ 893:164914

42. Zhang J, Ma C, Lang R, Sun L, Yang A, Li D (2023) Experimental study on mechanical properties of coastal remolded soft soil subjected to the freeze-thaw cycle under confining pressure. Rock Soil Mech 44(07):1863–1874

43. Zhang M, Pei W, Li S, Lu J, Jin L (2017) Experimental and numerical analyses of the thermo-mechanical stability of an embankment with shady and sunny slopes in a permafrost region. Appl Therm Eng 127:1478–1487

44. Zhang X, Ye P, Wu Y, Zhai E (2022) Experimental study on simultaneous heat-water-salt migration of bare soil subjected to evaporation. J Hydrol 609:127710

45. Zhang M, Zhang X, Lai Y, Lu J, Wang C (2018) Variations of the temperatures and volumetric unfrozen water contents of fine-grained soils during a freezing–thawing process. Acta Geotech 15(3):595–601

46. Zhao H, Wu Z, Li Z (2012) Experimental study on frost heave of silty clay in seasonally frost soil regions. Procedia Eng 28:282–286

47. Zhao HX, Zhong J, Wang ZJ (2014) Experimental study on the influence of different cooling rate to frost heave of silty clay. Adv Mater Res 912–914:136–140

48. Zhou J, Liang W, Meng X, Wei C (2021) Comparison of freezing and hydration characteristics for porous media. Permafrost Periglac 32(4):702–713

49. Zhou Z, Ma W, Zhang S, Mu Y, Li G (2018) Effect of freeze-thaw cycles in mechanical behaviors of frozen loess. Cold Reg Sci Tech 146:9–18

50. Zhou JS, Zhou GQ, Zhang Q, Liu ZQ, Zhao GS (2009) Experimental research on evolving rules of segregation ice in artificial frozen soil. Procedia Earth Planet Sci 1(1):544–549